Annu. Rev. Mater. Res. 2002. 32:77–111
doi: 10.1146/annurev.matsci.32.110101.155324

STATISTICAL DESCRIPTION OF MICROSTRUCTURES

S. Torquato
Department of Chemistry and Princeton Materials Institute, Princeton University, Princeton, New Jersey 08544; e-mail: torquato@princeton.edu

Key Words heterogeneous materials, amorphous materials, microstructure, statistical correlation functions, order metrics, topology

■ **Abstract** We review progress made in quantitatively ascertaining the various statistical correlation functions that are fundamental to determining the material properties of specific classes of disordered materials. Topics covered include the definitions of the correlation functions, a unified theoretical means of representing and computing the different statistical descriptors, structural characterization from two-dimensional and three-dimensional images of materials, scalar order metrics and particle packings, and reconstruction techniques.

INTRODUCTION

Structure, properties, performance, and processing constitute the key aspects of materials research. In this review article, we focus on the quantification of statistical correlation functions that are fundamental to determining the material properties of classes of disordered materials. Although space requirements prevent us from delving into the derivation of the structure/property relation themselves, we point out the connection between a specific correlation function and the macroscopic properties that depend upon it.

The ensuing analysis applies to several classes of materials, including random heterogeneous materials, amorphous many-body systems with spherically symmetric potentials, and materials with directional bonding (e.g., network glasses). Much of the discussion centers around the first two classifications.

By a heterogeneous material we mean a material that is composed of domains of different materials (phases), such as a composite, or the same material in different states, such as a polycrystal (1). Here the heterogeneity length scale is between hundreds of nanometers to several hundred microns. Heterogeneous materials abound in synthetic products and nature. Synthetic examples include aligned and chopped fiber composites, particulate composites, powders, interpenetrating multiphase composites cellular solids, colloids, gels, foams, phase-separated metallic alloys, microemulsions, block copolymers, and fluidized beds. Examples of natural heterogeneous materials are granular media, soils, polycrystals, sandstone, wood, bone, lungs, blood, animal and plant tissue, cell aggregates, and tumors.

In many instances, the microstructures can be characterized only statistically, and therefore such materials are referred to as random heterogeneous materials. A vast family of random microstructures are possible, ranging from dispersions with varying degrees of clustering to complex interpenetrating connected multiphase media, including porous media. Figure 1 shows examples of synthetic and natural random heterogeneous materials. The first example shows a processed optical image of a cermet that is primarily composed of boron carbide (black regions) and aluminum (white regions). Both of these phases are connected across the sample (interpenetrating) even though, from a planar section, it appears that only the black phase is connected. The second example shows a planar section through a Fontainebleau sandstone obtained via X-ray microtomography. As is seen below this imaging technique enables one to obtain full three-dimensional renderings of the microstructure, revealing that the void or pore phase (white region) is actually connected across the sample.

Amorphous many-body systems with spherically symmetric potentials represent another class of materials that we consider. At the molecular length scale, this classification includes metallic glasses. At length scales on the order of hundreds of nanometers and greater, this classification includes the special case of heterogeneous materials that consist of many interacting particles (e.g., colloids, powders, granular media, etc.). Figure 2 shows a random packing of spheres. In this article, we also remark on statistical descriptions of materials with directional bonding.

Disordered materials exhibit a remarkably broad spectrum of rich and complex microstructures. The goal is to develop a machinery to characterize statistically this broad class of microstructures, i.e., to develop a statistical, or stochastic, geometry

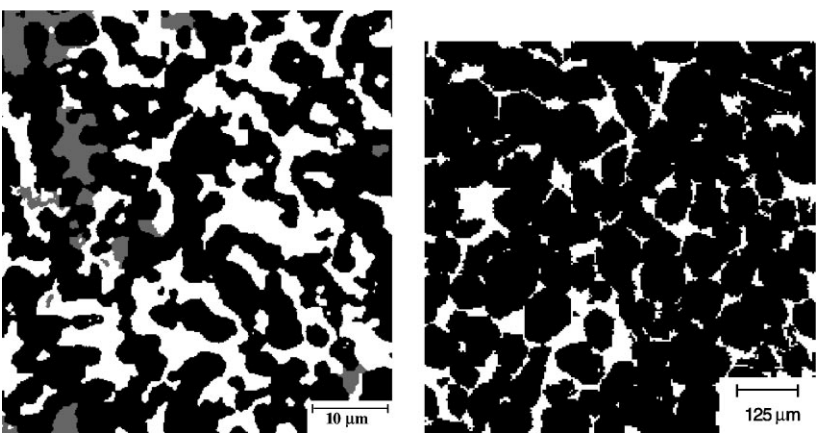

Figure 1 Examples of random heterogeneous materials. (*Left*) An interpenetrating three-phase cermet composed of boron carbide (*black regions*), aluminum (*white regions*), and another ceramic phase (*gray regions*) (2). (*Right*) Fontainebleau sandstone [data taken from (3)].

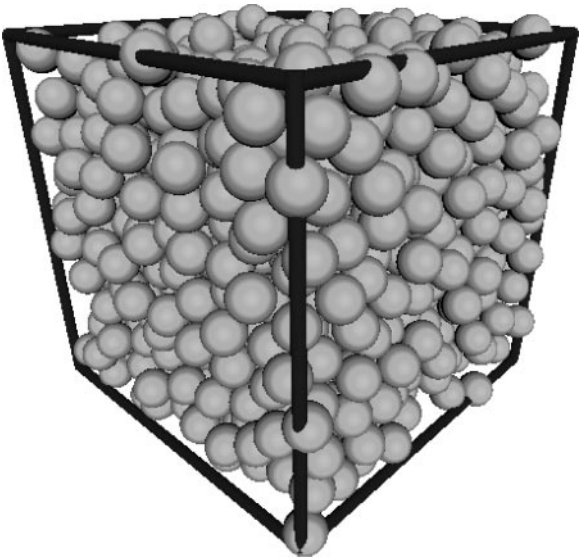

Figure 2 A realization of a random packing of 500 identical spheres near the maximally random jammed state obtained from the Lubachevsky-Stillinger simulation protocol.

of disordered materials. How or where does one begin to address this challenging task? The answer, of course, depends on what is the goal of the statistical characterization. Our goal is ultimately the prediction of the macroscopic or effective properties of the material, and thus this determines our starting point.

The diverse effective properties that we are concerned with here naturally and necessarily lead to a wide variety of microstructural descriptors, generically referred to as microstructural correlation functions. Invariably, such functions arise inside integrals in structure/property relations; more precisely, structure/property relations are functionals of the microstructural correlation functions (1).

STATISTICAL CORRELATION FUNCTIONS

We assume that the microstructures are static or can be approximated as static, and therefore any realization ω of the random material is taken to be independent of time. We speak in the language of heterogeneous materials because their possible morphologies and topologies are more general than molecular systems. In particular, we focus on two-phase heterogeneous materials.

Each realization ω of the two-phase random medium comes from some probability space and occupies some subset $\mathcal{V}$ of d-dimensional Euclidean space, i.e., $\mathcal{V} \in \Re^d$. The region of space $\mathcal{V} \in \Re^d$ of volume V is partitioned into two disjoint

random sets or phases: phase 1, a region $\mathcal{V}_1(\omega)$ of volume fraction ϕ_1, and phase 2, a region $\mathcal{V}_2(\omega)$ of volume fraction ϕ_2. Let $\partial\mathcal{V}(\omega)$ denote the surface or interface between $\mathcal{V}_1(\omega)$ and $\mathcal{V}_2(\omega)$. For a given realization ω, the indicator function $\mathcal{I}^{(i)}(\boldsymbol{x};\omega)$ for phase i for $\boldsymbol{x} \in \mathcal{V}$ is a random variable defined by

$$\mathcal{I}^{(i)}(\boldsymbol{x};\omega) = \begin{cases} 1, & \text{if } \boldsymbol{x} \in \mathcal{V}_i(\omega), \\ 0, & \text{otherwise}, \end{cases} \qquad 1.$$

for $i = 1, 2$. The indicator function $\mathcal{M}(\boldsymbol{x};\omega)$ for the interface is defined as

$$\mathcal{M}(\boldsymbol{x};\omega) = \left|\nabla\mathcal{I}^{(1)}(\boldsymbol{x};\omega)\right| = \left|\nabla\mathcal{I}^{(2)}(\boldsymbol{x};\omega)\right| \qquad 2.$$

and therefore is a generalized function (e.g., a function involving Dirac delta functions) that is nonzero when $\boldsymbol{x}$ is on the interface. Depending on the physical context, phase i can be a solid, fluid, or void characterized by some general tensor property. Unless otherwise stated, we drop ω from the notation and write $\mathcal{I}^{(i)}(\boldsymbol{x})$ for $\mathcal{I}^{(i)}(\boldsymbol{x};\omega)$ and $\mathcal{M}(\boldsymbol{x})$ for $\mathcal{M}(\boldsymbol{x};\omega)$.

In what follows, we define various statistical descriptors, the majority of which arise in structure/property relations. All of these microstructural functions have been evaluated for model microstructures and for real materials, some of which are described below in the sections Unified Theoretical Approach and Microstructure Characterization from Two-Dimensional and Three-Dimensional Images. The reader is referred to the book by Torquato (1) for specific references on such calculations.

n-Point Probability Functions

The so-called n-point probability function for phase i, $S_n^{(i)}$, is the the expectation of the product $\mathcal{I}^{(i)}(\boldsymbol{x}_1)\mathcal{I}^{(i)}(\boldsymbol{x}_2)\cdots\mathcal{I}^{(i)}(\boldsymbol{x}_n)$ (5), i.e.,

$$S_n^{(i)}(\boldsymbol{x}_1, \boldsymbol{x}_2, \ldots, \boldsymbol{x}_n) \equiv \left\langle \mathcal{I}^{(i)}(\boldsymbol{x}_1)\mathcal{I}^{(i)}(\boldsymbol{x}_2)\cdots\mathcal{I}^{(i)}(\boldsymbol{x}_n)\right\rangle. \qquad 3.$$

This quantity can be interpreted as the probability that n points at positions $\boldsymbol{x}_1, \boldsymbol{x}_2, \ldots, \boldsymbol{x}_n$ are found in phase i (1). For statistically homogeneous media, the $S_n^{(i)}$ are translationally invariant and therefore depend only on relative positions of the n points. In particular, $S_1^{(i)}(\boldsymbol{x}_1)$ is just the constant volume fraction ϕ_i of phase i. If the random medium is also statistically isotropic, the $S_n^{(i)}$ depend only on the distances between the n points. When possible, we suppress the superscript in $S_n^{(i)}$ that indicates phase i and simply denote the function by S_n. In such instances, the phase to which it refers is specified.

The n-point probability functions were introduced in the context of determining the effective transport properties of random media by Brown (6). These statistical descriptors arise in rigorous expressions (i.e., functionals) for the effective transport, electromagnetic, and mechanical properties of random heterogeneous media, including (*a*) effective conductivity, dielectric, magnetic permeability, and diffusion coefficient (6–10); (*b*) effective elastic moduli (7, 11–14); (*c*) trapping constant or, equivalently, mean survival time (15); and (*d*) fluid permeability (16–18).

The two-point or autocorrelation function $S_2(\boldsymbol{r}) \equiv \boldsymbol{S}_2^{(1)}(\boldsymbol{r})$ for statistically homogeneous media can be obtained by randomly tossing line segments of length $r \equiv |\boldsymbol{r}|$ with a specified orientation and counting the fraction of times the end points fall in phase 1 (see Figure 3). The function $S_2(\boldsymbol{r})$ provides a measure of how the end points of a vector $\boldsymbol{r}$ in phase 1 are correlated. For isotropic media, $S_2(r)$ attains its maximum value of ϕ_1 at $r = 0$ and eventually decays (usually exponentially fast) to its asymptotic value of ϕ_1^2. Debye & Bueche (19) showed that $S_2(r)$ for an isotropic porous solid can also be obtained via the intensity of scattered radiation.

Surface Correlation Functions

Surface correlation functions contain information about the random interface $\partial\mathcal{V}$ and are of basic importance in trapping and flow problems. In this context, we

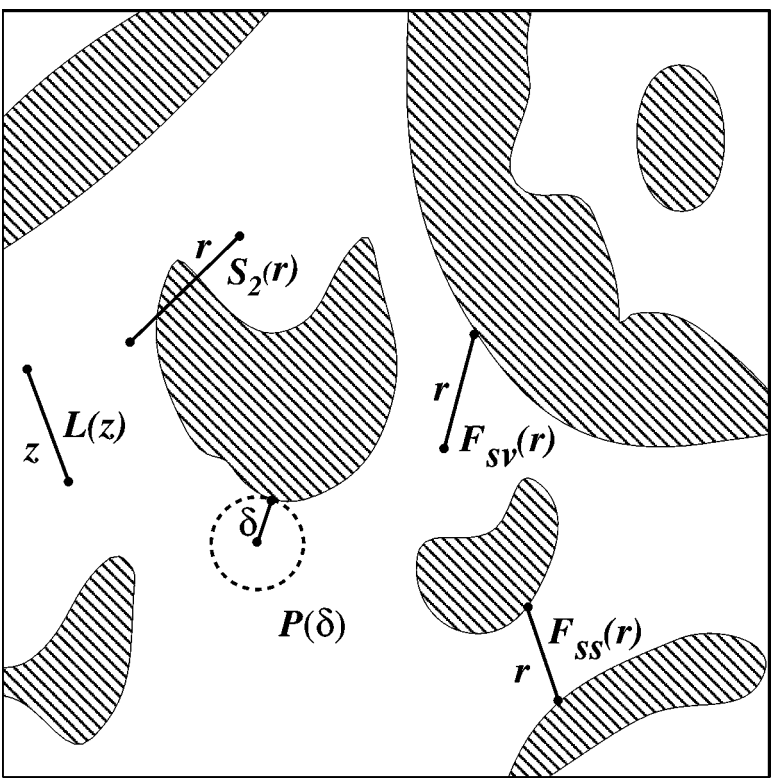

Figure 3 A schematic depicting events that contribute to lower-order functions for random media of arbitrary microstructure. Shown is the two-point probability function $S_2 \equiv S_2^{(1)}$ for phase 1 (*white region*), surface–void and surface–surface functions F_{sv} and F_{ss}, lineal-path function $L \equiv L^{(1)}$, and the pore-size density function P.

will let phase 1 denote the fluid or void phase, and phase 2 the solid phase. The simplest surface correlation function is the specific surface $s(\boldsymbol{x})$ (interface area per unit volume) at point $\boldsymbol{x}$, which is a one-point correlation function for statistically inhomogeneous media, i.e.,

$$s(\boldsymbol{x}) = \langle \mathcal{M}(\boldsymbol{x}) \rangle, \tag{4.}$$

where $\mathcal{M}(\boldsymbol{x})$ is the interface indicator function given by Equation 2. The nonnegative specific surface cannot be interpreted as a probability because the chance that a point at $\boldsymbol{x}$ lands on the interface is zero. For homogeneous media, it is a constant everywhere, which we denote simply by s.

Two-point surface correlation functions for statistically inhomogeneous media are defined by

$$F_{sv}(\boldsymbol{x}_1, \boldsymbol{x}_2) = \langle \mathcal{M}(\boldsymbol{x}_1)\, \mathcal{I}(\boldsymbol{x}_2) \rangle, \tag{5.}$$

$$F_{ss}(\boldsymbol{x}_1, \boldsymbol{x}_2) = \langle \mathcal{M}(\boldsymbol{x}_1)\, \mathcal{M}(\boldsymbol{x}_2) \rangle, \tag{6.}$$

where $\mathcal{I}(\boldsymbol{x}) \equiv \mathcal{I}^{(1)}(\boldsymbol{x})$ is the indicator function for the void phase. These functions are called the surface—void and surface—surface correlation functions, respectively, and they arise in rigorous bounds on the trapping constant (20, 21) and fluid permeability (18, 20) associated with fluid-saturated porous media. For statistically homogeneous media they depend only on the displacement $\boldsymbol{r} = \boldsymbol{x}_2 - \boldsymbol{x}_1$, and for isotropic media they depend only on the distance $r = |\boldsymbol{r}|$.

Lineal Measures

Another interesting and useful statistical measure is what we call the lineal-path function $L^{(i)}$ (22). For statistically isotropic media, $L^{(i)}(z)$ gives the probability that a line segment of length z lies wholly in phase i when randomly thrown into the sample. Figure 3 shows an event that contributes to the lineal-path function. We see that $L^{(i)}(z)$ contains a coarse level of connectedness information about phase i, albeit only along a lineal path of length z in phase i.

A quantity related to the lineal-path function $L^{(i)}(z)$ is the chord-length probability density function $p^{(i)}(z)$ (23, 24). They are related via the formula

$$p^{(i)}(z) = \frac{\ell_C}{\phi_i} \frac{d^2 L^{(i)}(z)}{dz^2}, \tag{7.}$$

where $\ell_C^{(i)}$ is the mean chord length for phase i defined by

$$\ell_C^{(i)} = \int_0^\infty z p^{(i)}(z)\, dz. \tag{8.}$$

The quantity $p^{(i)}(z)$ has also been called the chord-length distribution function. Chords are all of the line segments between intersections of an infinitely long line with the two-phase interface. For statistically isotropic media, the quantity $p^{(i)}(z)\, dz$ is the probability of finding a chord of length between z and $z + dz$ in phase i.

Because it is a probability density function (having dimensions of inverse length), $p^{(i)}(z) \geq 0$ for all z, and it normalizes to unity.

Knowledge of the chord-length density function is of basic importance in transport problems involving discrete free paths and thus has application in Knudsen diffusion and radiative transport in porous media (25–27). The function $p^{(i)}(z)$ has also been measured for sedimentary rocks (28) for the purpose of studying fluid flow through such porous media. Both $L^{(i)}(z)$ and $p^{(i)}(z)$ are quantities of great interest in stereology (29). For example, the mean chord (or intercept) length is the first moment of $p^{(i)}(z)$.

Pore-Size Functions

The pore-size probability density function $P(\delta)$ (also referred to as pore-size distribution function) first arose to characterize the void or pore space in porous media (30). Actually, $P(\delta)$ can be used to probe either phase 1 or phase 2 of general random media consisting of two material phases. For simplicity, we define $P(\delta)$ for phase 1, keeping in mind that it is equally well defined for phase 2. The quantity $P(\delta)$ for isotropic media is defined as the probability that a randomly chosen point in $\mathcal{V}_1(\omega)$ lies at a distance between δ and $\delta + d\delta$ from the nearest point on the pore-solid interface. Because it is a probability-density function (having dimensions of inverse length), $P(\delta) \geq 0$ for all δ and it normalizes to unity. At the extreme values of $P(\delta)$,

$$P(0) = \frac{s}{\phi_1}, \quad P(\infty) = 0, \tag{9.}$$

where s/ϕ_1 is the interfacial area per unit pore volume. The associated complementary cumulative distribution function $F(\delta) = \mathcal{P}\{\Delta \geq \delta\}$ (where Δ is the associated continuous random variable)

$$F(\delta) = \int_{\delta}^{\infty} P(r)\, dr \tag{10.}$$

is a nonincreasing function of δ such that

$$F(0) = 1, \quad F(\infty) = 0. \tag{11.}$$

Thus, $F(\delta)$ is the fraction of pore space that has a pore radius larger than δ.

Two-Point Cluster Function

Perhaps the most promising two-point descriptor identified to date is the two-point cluster function $C_2^{(i)}(\boldsymbol{x}_1, \boldsymbol{x}_2)$ (31). The quantity $C_2^{(i)}(\boldsymbol{x}_1, \boldsymbol{x}_2)$ gives the probability of finding two points at $\boldsymbol{x}_1$ and $\boldsymbol{x}_2$ in the same cluster of phase i. The formation of very large clusters of a phase in a heterogeneous material (on the order of the system size) can have a dramatic influence on its macroscopic properties. A cluster of phase i is defined as the part of phase i that can be reached from a point in phase i without passing through phase $j \neq i$. A critical point, known as the percolation

threshold, is reached when a sample-spanning cluster first appears. Thus, $C_2^{(i)}$ is the analogue of the two-point probability function $S_2^{(i)}$, but unlike its predecessor, it contains nontrivial topological "connectedness" information. Indeed, it is a useful signature of clustering in the system since it becomes longer ranged as the percolation threshold is approached from below. The measurement of $C_2^{(i)}$ for a three-dimensional material sample cannot be made from a two-dimensional cross-section of the material because it is an intrinsically three-dimensional microstructural function. The remaining challenge is to be able to incorporate $C_2^{(i)}$ into a theory to predict macroscopic properties for a wide range of conditions, even near the threshold.

Nearest-Neighbor Functions

All of the aforementioned statistical descriptors are defined for disordered materials of arbitrary microstructure. In the special case of random media composed of particles (phase 2) distributed randomly throughout another material (phase 1) or simple atomic systems, there is a variety of natural morphological descriptors. The description of the well-known n-particle probability density function ρ_n is discussed below in Unified Theoretical Approach. We describe some other functions below for systems of identical spherical particles of diameter D (or radius $R = D/2$) at number density ρ.

In considering a many-body system of interacting particles, a fundamental question is, What is the effect of the nearest neighbor on some reference particle in the system? The answer to this query requires knowledge of the probability associated with finding the nearest neighbor at some given distance from a reference particle, i.e., the particle nearest-neighbor probability-density function H_P. (This has been also called the nearest-neighbor distribution function.) Knowing H_P is of importance in a host of problems in the physical and biological sciences, including transport processes in heterogeneous materials (18, 21, 32), stellar dynamics (33), spatial patterns in biological systems (34), and the molecular physics of liquids and amorphous solids (35–39). Hertz (40) was the first to consider its evaluation for a system of spatially uncorrelated "point" particles, i.e., particles whose centers are Poisson distributed. The generalization of his result to d dimensions is given by

$$H_P(r) = \rho s_1(r) \exp[-\rho v_1(r)]. \qquad 12.$$

Here, $v_1(r)$ and $s_1(r) = dv_1/dr$ are the volume and surface area of a d-dimensional sphere of radius r, respectively (1). The calculation of H_P for spatially interacting particles is nontrivial.

A different nearest-neighbor function, H_V, arises in the scaled-particle theory of liquids (35, 41). This quantity (defined more precisely below) essentially characterizes the probability of finding a nearest-neighbor particle center at a given distance from an arbitrary point in the system. Since H_V is nontrivial when the point is located in the space exterior to the particles, we refer to it as the void nearest-neighbor probability-density function.

The quantity $H_V(r)\,dr$ gives the probability that at an arbitrary point in the system the center of the nearest particle lies at a distance between r and $r + dr$. Similarly, $H_P(r)\,dr$ gives the probability that at an arbitrary particle center in the system the center of the nearest particle lies at a distance between r and $r + dr$. Because both $H_V(r)$ and $H_P(r)$ are probability density functions, they are nonnegative for all r, normalize to unity, and have dimensions of inverse length. For statistically inhomogeneous media, $H_V(r)$ and $H_P(r)$ will depend also upon the position of the arbitrary point and the location of the central particle, respectively. Figure 4 shows an event that contributes to $H_P(r)$.

There are other nearest-neighbor quantities closely related to H_V and H_P that have been considered. These are the so-called exclusion probabilities E_V and E_P and the conditional pair distributions G_V and G_P. The interested reader is referred to the book by Torquato (1) for a detailed discussion of such related quantities.

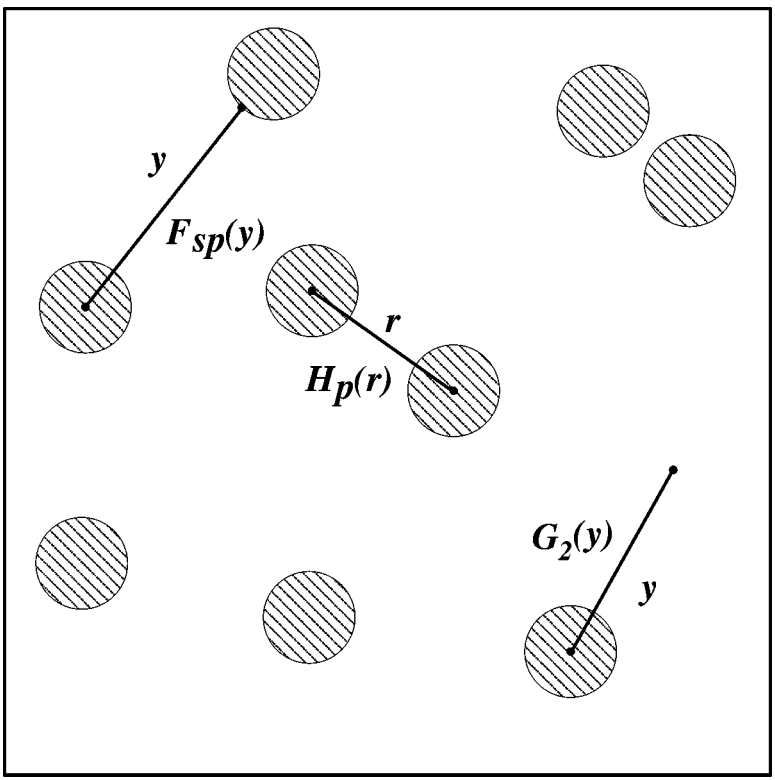

Figure 4 A schematic showing events that contribute to lower-order functions for random arrays of spheres (phase 2). Shown is the particle nearest-neighbor probability density H_P, point/particle function $G_2 \equiv G_2^{(1)}$, and the surface-particle function F_{sp}.

Point/q-Particle Correlation Functions

Consider statistically inhomogeneous media composed of N identical spherical particles of radius R (phase 2) distributed throughout another phase (phase 1). Let $\boldsymbol{r}^q \equiv \{\boldsymbol{r}_1, \ldots, \boldsymbol{r}_q\}$ denote the positions of q sphere centers and let $d\boldsymbol{r}^q \equiv d\boldsymbol{r}_1 d\boldsymbol{r}_2 \cdots d\boldsymbol{r}_q$. The point/$q$-particle correlation (or distribution) function $G_n^{(i)}(\boldsymbol{x}; \boldsymbol{r}^q)$ is defined such that $G_n^{(i)}(\boldsymbol{x}; \boldsymbol{r}^q)\, d\boldsymbol{r}^q$ gives the probability of finding a point in phase i at $\boldsymbol{x}$ and the center of a sphere in volume element $d\boldsymbol{r}_1$ about $\boldsymbol{r}_1$, the center of another sphere in volume element $d\boldsymbol{r}_2$ about $\boldsymbol{r}_2$, ..., and the center of another sphere in volume element $d\boldsymbol{r}_q$ about $\boldsymbol{r}_q$, where $n = 1 + q$. The point/q-particle correlation function arises in bounds on the effective conductivity (42), effective elastic moduli (43), trapping constant (21), and fluid permeability (18).

Surface-Particle Correlation Function

The surface/particle correlation function $F_{sp}(\boldsymbol{x}; \boldsymbol{r}_1)$ for statistically inhomogeneous systems of N identical spheres is the correlation function associated with a point being on the interface at $\boldsymbol{x}$ and the probability of finding the center of a sphere in volume element $d\boldsymbol{r}_1$ about $\boldsymbol{r}_1$. The surface/particle function F_{sp} arises in rigorous bounds on the fluid permeability of random beds of spheres (44) and the effective thermal conductivity of composites with imperfect interfaces (45).

UNIFIED THEORETICAL APPROACH

The previous section described some of the different types of statistical correlation functions that have arisen in rigorous structure/property relations (1). Until recently, application of such structure/property relations (although in existence for approximately 40 years in some cases) was virtually nonexistent because of the difficulty involved in ascertaining the correlation functions. Are these different functions related to one another? Can one write down a single expression that contains complete statistical information and thereby compute any specific correlation function? The key quantity that enables one to answer these two queries in the affirmative is the canonical n-point correlation function H_n (1, 46).

Canonical n-Point Correlation Function

For simplicity, we begin by considering a classical, closed system of N interacting identical spherical particles of radius R in volume V, keeping in mind that we can generalize the ensuing discussion to treat spheres with a polydispersivity in size, oriented nonspherical particles, and nonparticulate models such as cell models. We focus on microstructures that can be taken to be independent of time. In practice, this requirement restricts us to equilibrium systems or, more generally, quenched nonequilibrium systems. Any ensemble of many-particle systems is completely spatially characterized classically by the n-particle probability density

function $\rho_n(\boldsymbol{r}^n)$. The quantity $\rho_n(\boldsymbol{r}^n)\,d\boldsymbol{r}^n$ is proportional to the probability of finding any subset of n particles with configuration $\boldsymbol{r}^n$ in volume element $d\boldsymbol{r}^n$. Although ρ_n is not normalized to unity but rather

$$\int \rho_n(\boldsymbol{r}^n)\,d\boldsymbol{r}^n = \frac{N!}{(N-n)!}, \qquad 13.$$

it is still commonly referred to as a probability density function because it can be made so trivially by dividing it by the normalization constant $N!/(N-n)!$ The two-particle probability density ρ_2 can be ascertained from a scattering experiment via the structure factor (38). In general, $\rho_n(\boldsymbol{r}^n)\,d\boldsymbol{r}^n$ depends on the N-particle potential $\Phi_N(\boldsymbol{r}^N)$ and the particular dynamical process involved to create the system. In many instances, the total potential energy (in the absence of external fields) is well approximated by pairwise additivity, i.e.,

$$\Phi_N(\boldsymbol{r}^N) = \sum_{i<j}^{N} \varphi_2(r_{ij}), \qquad 14.$$

where $\varphi_2(r)$ is the pair potential.

The key idea employed by Torquato (46) to define and derive series representations of the canonical n-point correlation function H_n is the available space and available surface to the ith test particle of radius b_i that is inserted into the system of spheres of radius R. The available space and surface concepts go back to Boltzmann (47); see also (48), (49), and (50). The reader is referred to (46) and (1) for derivation of the series representations.

One representation of the H_n is given by

$$H_n(\boldsymbol{x}^m;\, \boldsymbol{x}^{p-m};\, \boldsymbol{r}^q) = \sum_{s=0}^{\infty} (-1)^s H_n^{(s)}(\boldsymbol{x}^m;\, \boldsymbol{x}^{p-m};\, \boldsymbol{r}^q), \quad n = p+q, \qquad 15.$$

where

$$H_n^{(s)}(\boldsymbol{x}^m;\, \boldsymbol{x}^{p-m};\, \boldsymbol{r}^q) = (-1)^m \frac{\partial}{\partial a_1} \cdots \frac{\partial}{\partial a_m} G_n^{(s)}(\boldsymbol{x}^p;\, \boldsymbol{r}^q),$$

$$G_n(\boldsymbol{x}^p;\, \boldsymbol{r}^q) = \sum_{s=0}^{\infty} (-1)^s G_n^{(s)}(\boldsymbol{x}^p;\, \boldsymbol{r}^q), \quad n = p+q,$$

$$G_n^{(s)}(\boldsymbol{x}^p;\, \boldsymbol{r}^q) = \frac{\prod_{l=1}^{q} \prod_{k=1}^{p} e(y_{kl};\, a_k)}{s!} \int \rho_{q+s}(\boldsymbol{r}^{q+s}) \prod_{j=q+1}^{q+s} m^{(p)}(\boldsymbol{x}^p;\, \boldsymbol{r}_j)\,d\boldsymbol{r}_j,$$

$$m^{(p)}(\boldsymbol{x}^p;\, \boldsymbol{r}_j) = 1 - \prod_{i=1}^{p} [1 - m(y_{ij};\, a_i)],$$

$$e(r;\, a) = 1 - m(r;\, a) = \Theta(r-a) = \begin{cases} 0, & r < a, \\ 1, & r \geq a, \end{cases}$$

$a_i = b_i + R$ and $y_{ij} = |\boldsymbol{x}_i - \boldsymbol{r}_j|$.

In many applications, we are interested in H_n in the limit that the radii of the test particles become zero so that $a_i = R$ for all i. For example, in this limit, the n-point matrix probability function is given by

$$S_n(\boldsymbol{x}^n) = \lim_{a_i \to R, \forall i} H_n(\emptyset; \boldsymbol{x}^n; \emptyset). \quad 16.$$

Similarly, the lower-order surface correlation functions are given by

$$s = \lim_{a_1 \to R} H_1(\boldsymbol{x}_1; \emptyset; \emptyset), \quad 17.$$

$$F_{sv}(\boldsymbol{x}_1, \boldsymbol{x}_2) = \lim_{a_i \to R, \forall i} H_2(\boldsymbol{x}_1; \boldsymbol{x}_2; \emptyset), \quad 18.$$

$$F_{ss}(\boldsymbol{x}_1, \boldsymbol{x}_2) = \lim_{a_i \to R, \forall i} H_2(\boldsymbol{x}_1, \boldsymbol{x}_2; \emptyset; \emptyset), \quad 19.$$

$$F_{sp}(\boldsymbol{x}_1, \boldsymbol{r}_1) = \lim_{a_1 \to R} H_2(\boldsymbol{x}_1; \emptyset; \boldsymbol{r}_1). \quad 20.$$

Three-point surface correlation functions (e.g., F_{ssv}, F_{ssp}, F_{svp}) and their n-point generalizations can be obtained from the H_n in a similar fashion. The point/q-particle correlation function is expressible as

$$G_n(\boldsymbol{x}_1; \boldsymbol{r}^q) = \lim_{a_1 \to R} H_n(\emptyset; \boldsymbol{x}_1; \boldsymbol{r}^q). \quad 21.$$

Using the formula for H_n, one can also establish relationships between these different types of correlation functions (46).

The void nearest-neighbor density function $H_V(r)$ (defined above in Nearest-Neighbor Functions) is a special case of H_n with $n = 1$, namely,

$$H_V(r) = H_1(\boldsymbol{x}_1; \emptyset; \emptyset), \quad 22.$$

where $a_1 = r$. Moreover, the particle nearest-neighbor density function $H_P(r)$ is given by

$$H_P(r) = -\frac{\partial E_P}{\partial r}, \quad 23.$$

where

$$E_P(r) = \lim_{|\boldsymbol{x}_1 - \boldsymbol{r}_1| \to 0} \frac{H_2(\emptyset; \boldsymbol{x}_1; \boldsymbol{r}_1)}{\rho_1(\boldsymbol{r}_1)} \quad 24.$$

and $a_1 = r$.

Other Model Microstructures

Representations of the H_n for dispersions of spheres with a size distribution have also been obtained (51). The formal results described above extend to statistically anisotropic models consisting of inclusions whose configuration is fully specified by center-of-mass coordinates (e.g., oriented ellipsoids, cubes, cylinders, squares,

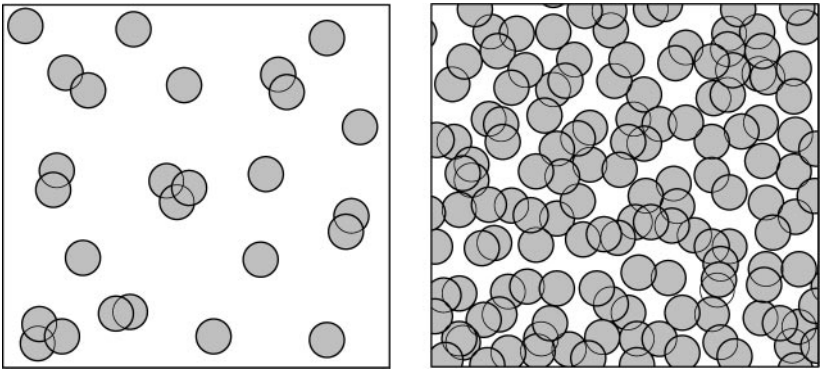

Figure 5 Two-dimensional overlapping-particle systems at a low density with at most three particle overlaps (*left*) and at a high density above the percolation threshold (*right*).

etc.) (52), as well as to statistically anisotropic laminates (53). The formalism also extends to nonparticulate systems, such as cell or lattice models (1, 54).

Model Pair Potentials

For a system of noninteracting particles, we have that $\varphi_2 = 0$ and thus $\Phi_N = 0$. In so far as statistical thermodynamics is concerned, this is the trivial case of an ideal gas. However, this is also a nontrivial model of a heterogeneous material because the lack of spatial correlation implies that the particles may overlap to form complex clusters, as shown in Figure 5. At low-sphere densities, the particle phase is a dispersed, disconnected phase, but above a critical value, called the percolation threshold, the particle phase becomes connected. For $d = 2$ and $d = 3$, this threshold occurs at a sphere volume fraction of approximately 0.68 and 0.29, respectively (1). We refer to this model as overlapping spheres. Interpenetrable-sphere systems in general are useful models of consolidated media, such as sandstones and other rocks, and sintered materials.

In the hard-sphere pair potential, the particles do not interact for interparticle separation distances greater than the sphere diameter D but experience an infinite repulsive force for distances less than or equal to D, i.e.,

$$\varphi_2(r) = \begin{cases} +\infty, & r \leq D, \\ 0, & r > D. \end{cases} \qquad 25.$$

Hard-sphere systems have received considerable attention because they serve as a useful model for a number of physical systems, such as simple liquids (35, 55, 56), glasses (38), colloidal dispersions (57), fiber-reinforced composites (58), particulate composites (59), and granular media (60). The hard-sphere model approximates well the structure of dense-particle systems with more complicated potentials

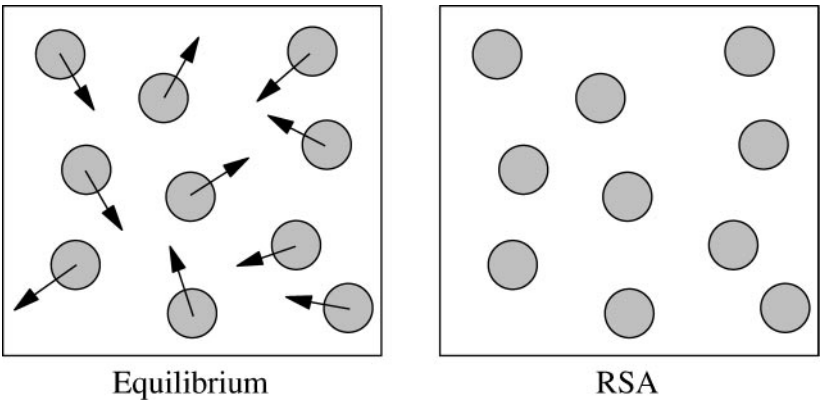

Figure 6 Snapshot of an equilibrium system of hard particles (*left*) and a realization of hard particles assembled according to an RSA process (*right*). In the former, the particles are free to sample the configuration space subject to impenetrability of the other particles, but in the latter the particles are frozen at their initial positions.

(e.g., the Lennard–Jones model discussed below) because short-range repulsion between the particles is the primary factor in determining the spatial arrangement of the particles.

For hard-sphere systems, the impenetrability constraint does not uniquely specify the statistical ensemble. The hard-sphere system can be in thermal equilibrium or in one of the infinitely many nonequilibrium states, such as the random sequential addition (or adsorption) (RSA) process (see Figure 6). The latter is produced by randomly, irreversibly, and sequentially placing nonoverlapping objects into a volume (61). For identical d-dimensional RSA spheres, the filling process terminates at the saturation limit, which is substantially lower than the maximum density for random hard spheres in equilibrium. Denoting the maximum sphere volume fraction by $\phi_2^{\max}$, it turns out that for identical hard spheres in an RSA process in the thermodynamic limit, $\phi_2^{\max} \approx 0.75$, 0.55, and 0.38 for $d = 1$, 2, and 3, respectively (62–64). In contrast, for identical disordered hard spheres in equilibrium, $\phi_2^{\max}$ is exactly unity for $d = 1$, and for $d = 2$ and 3, $\phi_2^{\max} \approx 0.83$ and 0.64, respectively (1). Unlike what we see in the case of overlapping spheres, the n-particle probability density function ρ_n for general ensembles of hard spheres is nontrivial.

Interpenetrable-sphere models enable one to define systems that are intermediate between overlapping spheres and impenetrable spheres, thereby allowing one to vary degree of connectivity of the particle phase. A popular interpenetrable-sphere model is the penetrable-concentric-shell model or, more colloquially, the cherry-pit model. The pair potential is given by

$$\varphi_2(r) = \begin{cases} +\infty, & r \le \lambda D, \\ 0, & r > \lambda D. \end{cases} \qquad 26.$$

When $0 \le \lambda \le 1$, each sphere of diameter D may be thought of as being composed

of an impenetrable core of diameter λD encompassed by a perfectly penetrable concentric shell of thickness $(1-\lambda)D/2$. By varying the impenetrability parameter λ between 0 and 1, one can continuously pass between fully penetrable (overlapping) spheres and totally impenetrable spheres, respectively.

Well-known models that incorporate attractive interactions include the square-well potential and the Lennard-Jones potential (55). A special limit of the square-well potential that reduces attractive interactions to a delta function at contact is referred to as the sticky hard-sphere potential proposed by Baxter (65). This potential provides a simple means of modeling aggregation processes in particle systems.

Illustrative Calculations

Given the series representation of the canonical n-point correlation function H_n, one can compute (using statistical-mechanical techniques) specific statistical descriptors as special limiting cases as outlined above. Here we report a few illustrative calculations of correlation functions. The reader is referred to Torquato (1) for computational details.

Figure 7 shows the matrix two-point probability function S_2 for three-dimensional overlapping spheres (phase 2) at a sphere volume fraction $\phi_2 = 0.5$. Included in

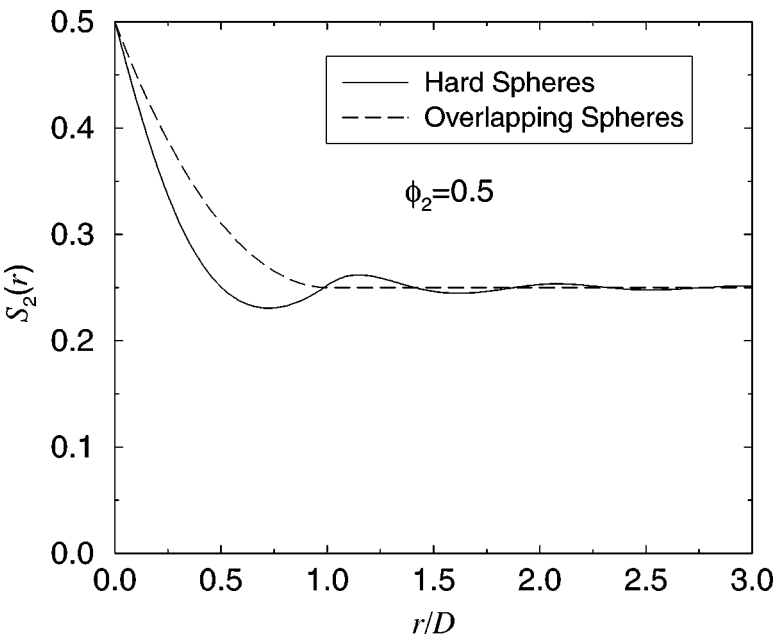

Figure 7 The matrix two-point probability function $S_2(r)$ versus the dimensionless distance r/D for two models of isotropic distributions of spheres of diameter $D = 2R$ at a sphere volume fraction $\phi_2 = 0.5$ (66, 67).

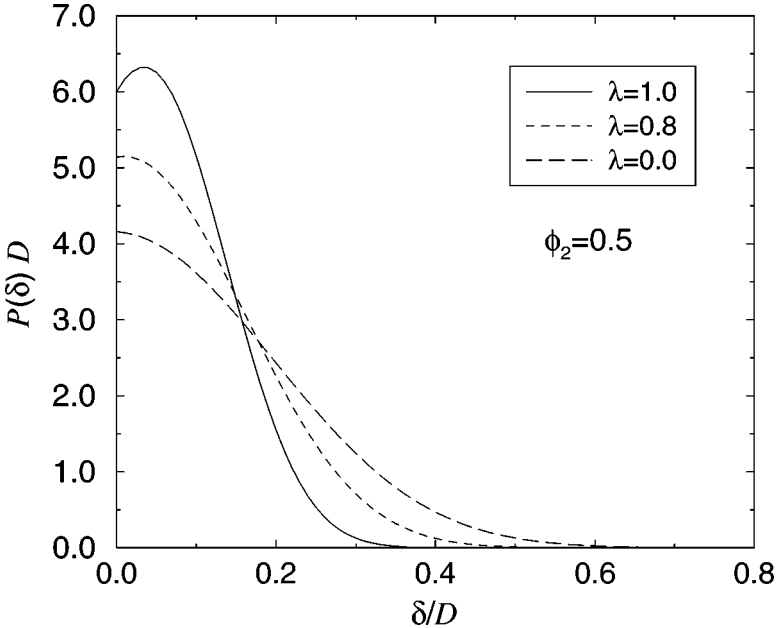

Figure 8 The pore-size density function $P(\delta)$ versus the dimensionless distance δ/D for equilibrium spheres of radius $R = D/2$ in the cherry-pit model for three different values of the impenetrability parameter λ (68).

the figure is the corresponding plot of S_2 for equilibrium hard (totally impenetrable) spheres, which, unlike overlapping spheres, exhibit short-range order.

Figure 8 shows the pore-size density function $P(\delta)$ for in the cherry-pit model for three different values of the impenetrability parameter λ: $\lambda = 0$ (overlapping spheres), $\lambda = 0.8$, and $\lambda = 1$ (totally impenetrable spheres). Consistent with the fact that there are greater spatial fluctuations in the pore size as λ is made smaller, we see that the "tail" of $P(\delta)$ increases with decreasing λ.

Figure 9 shows the two-point cluster function C_2 for sticky hard spheres. The key point is that C_2 becomes longer ranged as the percolation threshold $\phi_{2c} = 0.297$ is approached from below.

MICROSTRUCTURE CHARACTERIZATION FROM TWO-DIMENSIONAL AND THREE-DIMENSIONAL IMAGES

The measurement of correlation functions from images of real materials has evolved considerably since the work of Corson (69, 70), who used an unautomated painstaking procedure to compute three-point functions from photographs of cross-sections of heterogenous materials. There now exist a variety of methods to

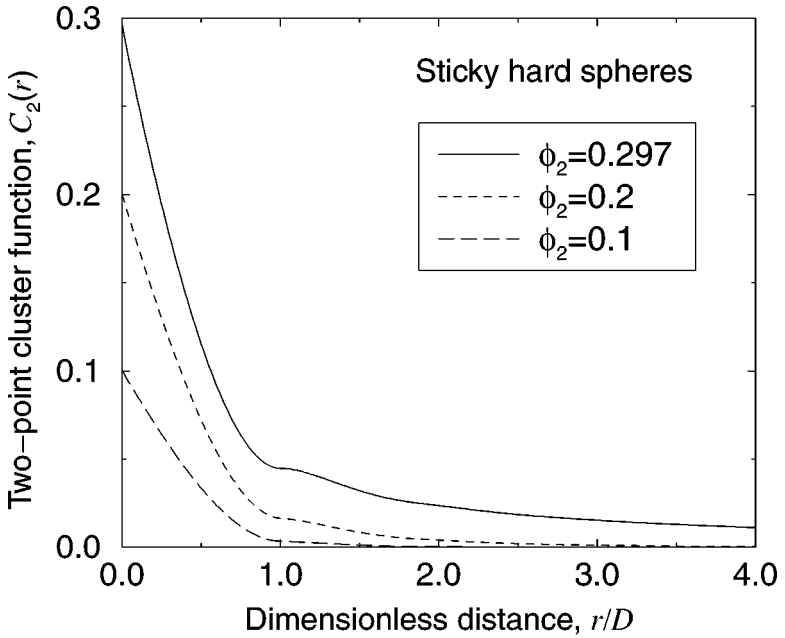

Figure 9 Two-point cluster function $C_2(r)$ versus the dimensionless distance r/D for sticky hard spheres of diameter D at several values of the sphere volume fraction ϕ_2. Here $\tau = 0.35$ is the dimensionless stickiness parameter and $\phi_{2c} = 0.297$.

obtain two- and three-dimensional images of heterogeneous materials, including transmission electron microscopy (71), scanning tunneling electron microscopy (72), synchrotron-based tomography (73), magnetic resonance imaging (74), and confocal microscopy (75). Although electron-microscopic techniques only provide two-dimensional images, X-ray–tomographic, magnetic-resonance-imaging, and confocal-microscopic techniques provide full three-dimensional images of materials. All of these imaging methods are nonintrusive, leaving the sample intact and unaltered.

Figure 10 shows two different representations of the same three-dimensional digitized data set ($128 \times 128 \times 128$ pixels) of a portion of a Fontainebleau sandstone (76). Each pixel is a cubic region of size $7.5 \times 7.5 \times 7.5$ μm^3. The full data set ($512 \times 512 \times 512$ pixels) was obtained via X-ray microtomography (3). The figure depicts the complex three-dimensional pore space as well as a three-dimensional perspective of corresponding surface cuts through the sample.

Digitized representations of the samples are utilized to analyze images on the computer. One must analyze two- or three-dimensional arrays of gray values spanning the finite system, typically subjected to periodic boundary conditions. For a two-phase material, the gray-scale image can be reduced to a binary image by operations such as thresholding, in which gray values lighter than a chosen threshold are set to white and the others set to black. The image is thus reduced to an array of

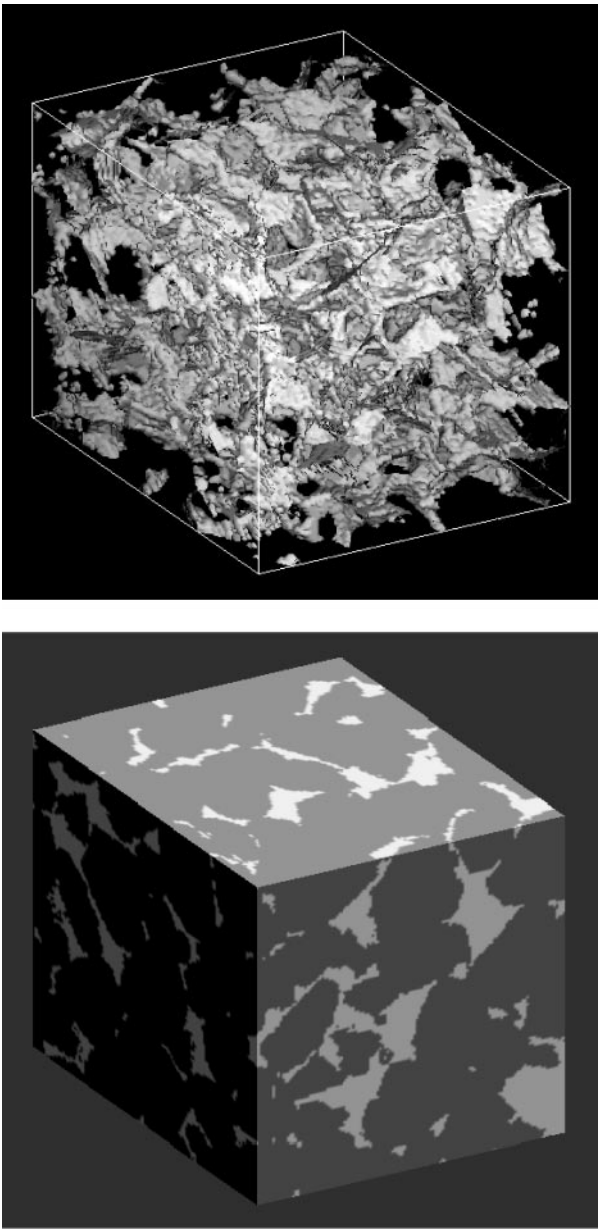

Figure 10 (*Left*) The pore space of a 128 × 128 × 128 pixel subregion of a Fontainebleau sandstone obtained via X-ray microtomography (each pixel has volume 7.5 × 7.5 × 7.5 μm^3) (76). The pore space is white and opaque, and the grain phase is black and transparent. (*Right*) Three-dimensional perspective of surface cuts of the same subregion.

bits or pixels (voxels). The same procedure can be applied to multiphase media. In practice, one often has only a single digitized image to analyze (not an ensemble of them). In such instances, the system size must be sufficiently larger than the correlation length of interest in order for meaningful statistics to be extracted.

The two-point probability function $S_2(\boldsymbol{r})$ can be computed using a sampling template (77). Figure 11 shows this function for the aforementioned sandstone. For

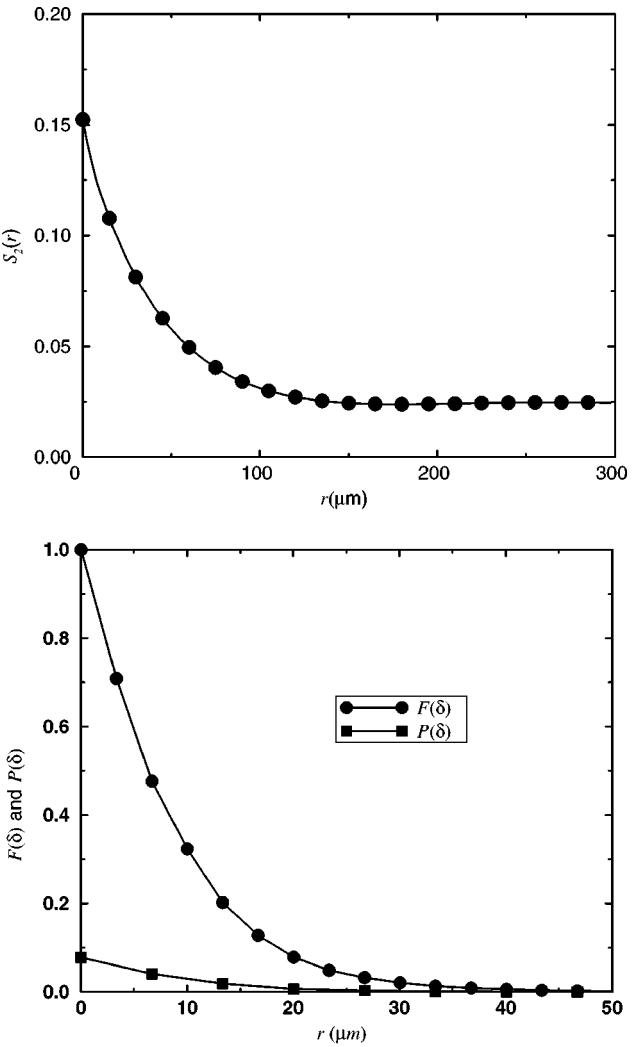

Figure 11 Some statistical descriptors of the for Fontainebleau sandstone shown in Figure 10. (*Left*) Two-point probability function $S_2(r)$ for the void phase. (*Right*) Pore-size density function $P(\delta)$ and complementary cumulative distribution function $F(\delta)$.

statistically isotropic samples, both the two- and three-point probability functions, S_2 and S_3, respectively can be computed from a planar section through the material. For an isotropic digitized system, there is a superior way to compute $S_2(r)$ (78), namely, to sample in only a few select directions. Another way to compute $S_2(\boldsymbol{r})$ is to utilize its spectral representation and efficient fast Fourier transform techniques (79). Berryman has used image processing techniques to obtain S_2 of synthetic and real porous materials (80, 81). Specifically, he measured S_2 and estimated s of glass-bead samples and of sandstones. Moreover, he has devised an efficient means of obtaining and visualizing the three-point probability function S_3 (82). Similar techniques have been used to calculate lineal measures, such as the lineal-path function $L(z)$ and chord-length density function $p(z)$ (3).

Unlike many of the previous quantities, the pore-size density function $P(\delta)$ is an intrinsically three-dimensional microstructural function and hence cannot be obtained from a two-dimensional slice. Therefore, it must be determined from a full three-dimensional digitized sample. The pore-size density function is obtained by binning the sphere radii found in the second step and dividing by the total number of radii. Figure 11 shows both $P(\delta)$ and $F(\delta)$ for the void phase of the Fontainebleau sandstone (3).

The two-point cluster function $C_2(r)$ is computed in the same manner as $S_2(r)$, except that one must determine when the end points of the line segment of length r fall in the same cluster of phase 1 (phase 2). First, one must establish a criterion that defines when two pixels are connected (e.g., a nearest-neighbor connectivity rule), and then cluster identification algorithms (83, 84) can be used. Armed with such information, one could also compute other cluster statistics (1).

SCALAR ORDER METRICS AND PARTICLE PACKINGS

There is a well-developed theoretical and experimental framework available for characterizing the structure of regular crystalline solids (85). By contrast, the quantification of the structure of amorphous materials is much less well understood, despite the fact that many natural and synthetic materials exhibit disorder on a variety of different length scales. Examples range from liquids, gases, and amorphous solids to porous rocks, dispersions, soil, and biological materials such as tissue. In such systems, it is natural to ask the following question: To what extent can we quantify the degree of order (or disorder) present in the sample? Clearly, the aforementioned statistical correlation functions contain the information required to answer this question. However, for pragmatic purposes, it is desirable to develop sensitive scalar measures of order that we refer to as order metrics.

Central to the notion of characterizing disorder is understanding the relative placement of different materials in some relevant order parameter space. At one extreme, a truly random system should exhibit no positional, orientational, or conformational correlations; i.e., its structure is that of an ideal gas. At the opposite extreme, a regular crystalline array is a manifestation of perfect order. Between

the ideal gas and the perfect crystal lie imperfect gases, liquids (both stable and metastable), glasses, defective crystals, and structures that evolve from nonequilibrium processes, such as irreversible adsorption onto a surface. All such systems exhibit a certain degree of order (or disorder), and the differences between them can be quite subtle. For instance, the classic problem of distinguishing between the structures of dense glasses and polycrystalline materials remains a significant challenge to materials scientists and engineers (38, 86).

Maximally Random Jammed State

Bernal (87) has remarked that "heaps (random close-packed arrangements of particles) were the first things that were ever measured in the form of basketfuls of grain for the purpose of trading or of collection of taxes." Random packings of hard spheres serve as the starting point to understand the structure of living cells, liquids, granular media, and glasses, to mention but a few examples. Despite the apparent simplicity of the hard-sphere model, there exist subtle fundamental concepts concerning its structure that remain to be elucidated. One of these came to light explicitly in a recent paper by Torquato et al. (4). Those authors showed that the venerable concept of the random close packed state (RCP) is mathematically ill-defined. This explains why, to this day, there is no rigorous prediction of the RCP density, although such attempts have been made (88, 89). The old idea of the RCP state was based upon the notion that there should be a randomly arranged analog of the crystalline closed-packed state. Accordingly, the RCP density was thought to be the highest density that a random packing of particles could attain. The term close packed implies maximal coordination throughout the system, i.e., an ordered lattice, which clearly is in conflict with the notion of randomness. The exact proportion of these two competing effects is not well-defined, and therein lies the problem. Finally, the notion of the randomness was never quantified, nor even clearly defined.

To quantify the order (or disorder) in jammed sphere systems, Torquato et al. (4) chose to examine two simple but fundamentally important measures of order: bond-orientational order and translational order. The first is obtainable in part from the metric Q_6, and the second is obtainable in part from the radial distribution function $g_2(r)$. To each nearest-neighbor bond emanating from a sphere for $d = 3$, one can associate the spherical harmonics $Y_{lm}(\theta, \varphi)$ using the bond angles as arguments. Then Q_6 is defined by (90)

$$Q_6 \equiv \left(\frac{4\pi}{13} \sum_{m=-6}^{6} \left| \overline{Y_{6m}} \right|^2 \right)^{1/2}, \qquad 27.$$

where $\overline{Y_{6m}}$ denotes an average over all bonds. For a completely disordered system in the infinite-volume limit, Q_6 equals zero, whereas Q_6 attains its maximum value for space-filling structures ($Q_6^{\mathrm{FCC}} \approx 0.575$) in the perfect FCC crystal. Thus, Q_6 provides a global measure of FCC crystallite formation in the system. For

convenience, we normalize the orientational order metric by its value in the perfect FCC crystal, i.e., $Q \equiv Q_6/Q_6^{\mathrm{FCC}}$.

Scalar measures of translational order have not been well studied. Torquato et al. (4) have introduced a simple translational order metric T that measures the degree of spatial ordering relative to the perfect FCC lattice at the same volume fraction. Specifically,

$$T = \left| \frac{\sum_{i=1}^{N_C} \left(n_i - n_i^{\mathrm{ideal}}\right)}{\sum_{i=1}^{N_C} \left(n_i^{\mathrm{FCC}} - n_i^{\mathrm{ideal}}\right)} \right|, \qquad 28.$$

where n_i, for the system of interest, denotes the average occupation number for the shell of width $a\delta$ centered at a distance from a reference sphere that equals the ith nearest-neighbor separation for the open FCC lattice at that density. Moreover, a is the first nearest-neighbor distance for that FCC lattice, and N_C is the total number of shells. Similarly, n_i^{ideal} and n_i^{FCC} are the corresponding shell occupation numbers for an ideal gas (spatially uncorrelated spheres) and the open FCC lattice. Observe that $T = 0$ for an ideal gas (perfect randomness), and $T = 1$ for perfect FCC spatial ordering.

Both Q and T are crystal-dependent measures in that they measure order with respect to the FCC lattice. Other reasonable choices for order metrics have been tested, including crystal-independent ones, such as an information-theoretic entropy and another translational-order metric. Importantly, the evaluations of these order metrics resulted in the same qualitative behavior as that given by Q and T for the configurations discussed immediately below. All of these results, as well as the utility of other, more sophisticated order metrics for many-particle systems in general, have been described elsewhere (91–93).

To assess the validity of the RCP state, Torquato et al. (4) carried out molecular dynamics simulations using systems of 500 identical hard spheres with periodic boundary conditions. Starting from an equilibrium liquid configuration at a packing fraction $\eta \equiv \phi_2$ equal to 0.3, they compressed the system to a jammed state by the well-known method of Lubachevsky & Stillinger (94), which allows the diameter of the particles to grow linearly in time with a dimensionless rate Γ. The jammed state occurs when the diameters can no longer increase in time, the sphere collision rate diverges, and no further compression can be achieved after relaxing the configuration at the jammed packing fraction. Figure 12 shows that the packing fraction of the final jammed states is inversely proportional to the compression rate Γ. A linear extrapolation of the data to the infinite compression rate limit yields $\eta \approx 0.64$, which is close to the supposed RCP value reported by Scott & Kilgour.

Figure 12 also shows their results for the aforementioned jammed structures in the Q-T plane. The key point is that the degree of order increases monotonically with the jammed packing fraction. These results demonstrate that the notion of RCP as the highest possible density that a random sphere packing can

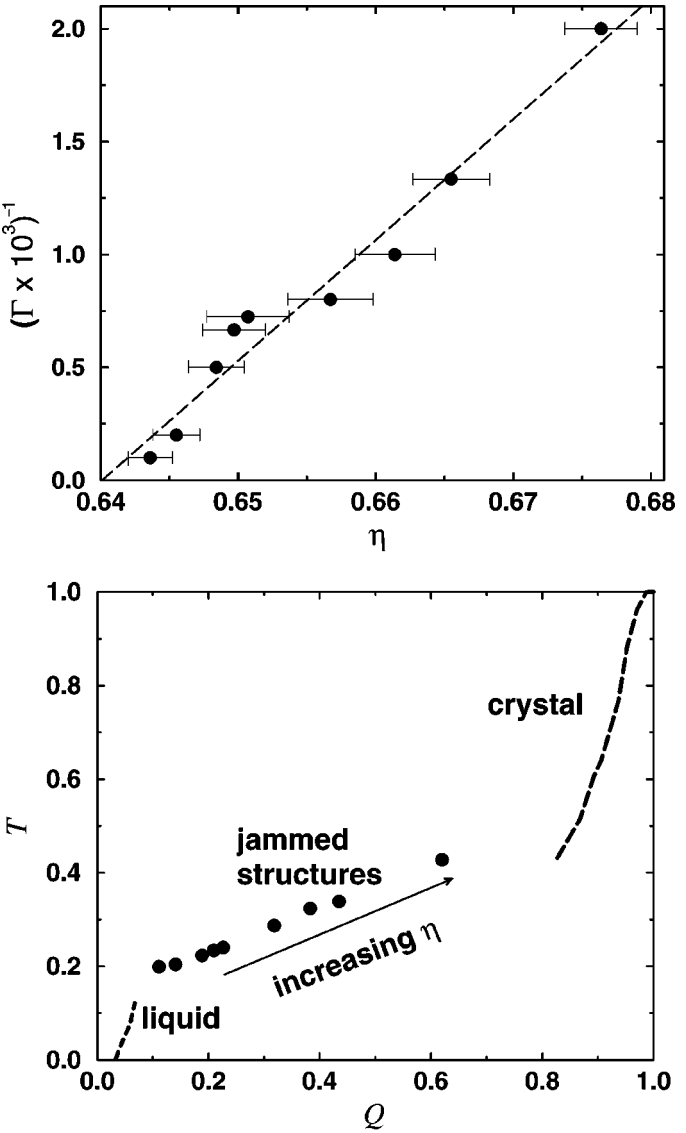

Figure 12 (*Left*) The reciprocal compression rate Γ^{-1} versus the packing fraction η of the final jammed state of hard spheres using the molecular dynamics compression protocol of Lubachevsky & Stillinger (94). (*Right*) The *Q*-*T* plane for the hard-sphere system, where *T* and *Q* are translational and orientational order metrics, respectively. Shown are the average values for the jammed states, as well as states along the equilibrium liquid (*dotted*) and crystal (*dashed*) branches.

attain is ill-defined because one can achieve packings with arbitrarily small increases in packing fraction at the expense of small increases in order. Note that the MRJ packing fraction η_M is approximately equal to 0.64 for 500-sphere systems using the Lubachevsky–Stillinger protocol. However, this cannot be considered a true estimate of η_M because other protocols may indeed find jammed states with a lower degree of order as measured by Q or some other order metric.

To summarize, the notion of the RCP state is not well-defined mathematically. To replace this idea, a new concept has been introduced: the maximally random jammed state, which can be defined precisely once an order metric ψ is chosen. This lays the mathematical groundwork for studying randomness in packings of particles and initiates the search for the MRJ state in a quantitative way not possible before. Nevertheless, significant challenges remain. First, new and efficient protocols (both experimental and computational) that generate jammed states must be developed. Second, since the characterization of randomness in sphere packings is in its infancy, the systematic investigation of better order metrics is crucial. In a recent study (93), a comprehensive set of candidate jammed states of identical hard spheres (generated via computer simulations) and a variety of different order metrics have been used to estimate the MRJ packing fraction to be $\eta_M = 0.637 \pm 0.0015$. The determination of the maximally random jammed state for systems of spheres with a polydispersivity in size and for systems of ellipsoids are intriguing open problems, not to mention the determination of MRJ states for such packings.

Molecular Systems

The quantification of order in terms of scalars enables one to place the equilibrium and nonequilibrium (or history-dependent) states of molecular systems in order metric space. This has recently led to valuable insights into the molecular nature of systems of atoms with spherically symmetric potentials (91) as well as systems with orientation-dependent interactions, such as water (95). Nonetheless, the use of order metrics to characterize materials of the latter category (those with directional bonding) is a fertile area for research. For example, network glasses (see Figure 13) have not been analyzed in this fashion. One could imagine the development of order metrics for network glasses that involve ring statistics, the pair correlation function, and bond-angle distributions (38).

RECONSTRUCTION TECHNIQUES

The reconstruction of realizations of disordered materials from a knowledge of limited microstructural information (lower-order correlation functions) is an intriguing inverse problem. Clearly, one can never reconstruct the original material perfectly, i.e., such reconstructions are nonunique. Thus, the objective here is not

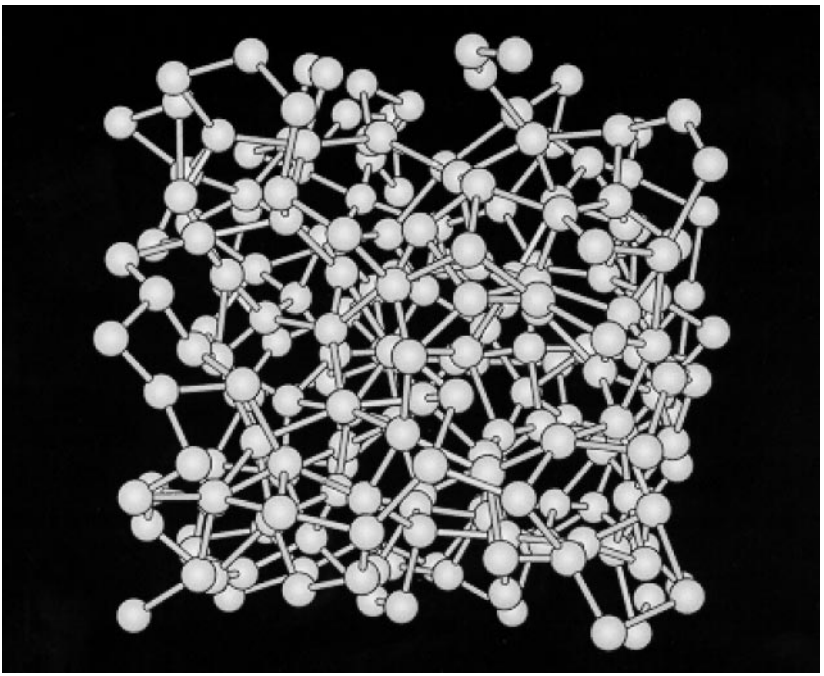

Figure 13 A schematic representation of a network glass.

the same as that of data decompression algorithms that efficiently restore complete information, such as the gray-scale of every pixel in an image.

The generation of realizations of random media with specified lower-order correlation functions can

1. shed light on the nature of the information contained in the various correlation functions that are employed;
2. ascertain whether the standard two-point probability function S_2, accessible experimentally via scattering, can accurately reproduce the material and, if not, what additional information is required to do so;
3. attempt to reconstruct the full three-dimensional structure of the heterogeneous material from lower-order information extracted from two-dimensional plane cuts through the material: a problem of great practical value, since one often has only two-dimensional information, such as a micrograph or planar image;
4. identify the class of microstructures that have exactly the same lower-order correlation functions but widely different effective properties;
5. probe the interesting issue of nonuniqueness of the generated realizations;

6. construct structures that correspond to specified correlation functions and categorize classes of random media; and
7. provide guidance in ascertaining the mathematical properties that physically realizable correlation functions must possess (96).

The first reconstruction procedures were based on thresholding Gaussian random fields. The theory of the statistical topography of Gaussian random fields was originally established in the work of Rice (97). One approach to reconstructing random media originated with Joshi (98) and was extended by Quibler (99) and Adler (100). Another related approach originated with Cahn (101) and was later extended (102–104). Both approaches are currently limited to the two-point probability function S_2. In addition, such methods are not suitable for extension to non-Gaussian statistics, and hence are model dependent, i.e., depend on the underlying Gaussian statistics.

Optimization Problem

It has recently been suggested that reconstruction problems can pose as optimization problems (78, 105). A set of target correlation functions are prescribed based upon experiments, theoretical models or some ansatz. Starting from some initial realization of the random medium, the method proceeds to find a realization by evolving the microstructure such that the calculated correlation functions best match the target functions. This is achieved by minimizing an error based upon the distance between the target and calculated correlation functions. The medium can be an amorphous system of atoms (105) or, more generally, a digitized image (78).

For simplicity, we focus on digitized media and consider only a single two-point correlation function $f_2(r)$ for statistically isotropic two-phase media. (The generalization to multiple correlation functions is straightforward (78, 105).) It is desired to generate realizations of two-phase isotropic media that have a target two-point correlation function $f_2(r)$ associated with phase i, where r is the distance between the two points. Let $\hat{f}_2(r)$ be the corresponding function of the reconstructed digitized system (with periodic boundary conditions) at some time step. It is this system that we attempt to evolve toward $f_2(r)$ from an initial guess of the system realization. Again, for simplicity, we define a fictitious energy (or norm-2 error) E at any particular stage as

$$E = \sum_r \left[\hat{f}_2(r) - f_2(r) \right]^2, \qquad 29.$$

where the sum is over all discrete values of r. Potential candidates for the correlation functions (1) include (a) two-point probability function $S_2^{(i)}(r)$, lineal path function $L^{(i)}(z)$, pore-size density function $P^{(i)}(\delta)$, and (b) two-point cluster function $C_2^{(i)}(r)$.

Solution of Optimization Problem

The aforementioned optimization problem is very difficult to solve due to the complicated nature of the objective function, which involves complex microstructural information in the form of correlation functions of the material, and due to the combinatorial nature of the feasible set. Standard mathematical programming techniques are therefore most likely inefficient and likely to get trapped in local minima. In fact, the complexity and generality of the reconstruction problem make it difficult to design any deterministic algorithms of wide applicability (for example, see (106)). We therefore resort to heuristic techniques for global optimization, in particular, the simulated annealing method.

Simulated annealing has been applied successfully to many difficult combinatorial problems, including NP-hard ones such as the "traveling salesman" problem. The utility of the simulated annealing method stems from its simplicity in that it only requires "black-box" cost function evaluations, and in its physically designed ability to escape local minima via accepting locally unfavorable configurations. In its simplest form, the states of two selected pixels of different phases are interchanged, automatically preserving the volume fraction of both phases. The change in the error (or energy) $\Delta E = E' - E$ between the two successive states is computed. This phase interchange is then accepted with some probability $p(\Delta E)$ that depends on ΔE. One reasonable choice is the Metropolis acceptance rule, i.e.,

$$p(\Delta E) = \begin{cases} 1, & \Delta E \leq 0, \\ \exp(-\Delta E/T), & \Delta E > 0, \end{cases} \qquad 30.$$

where T is a fictitious temperature. The concept of finding the lowest error (lowest energy) state by simulated annealing is based on a well-known physical fact: If a system is heated to a high temperature T and then slowly cooled down to absolute zero, the system equilibrates to its ground state.

There are various ways of appreciably reducing computational time. For example, computational cost can be significantly lowered by using other stochastic optimization schemes such as the Great Deluge algorithm, which can be adjusted to accept only downhill energy changes, and the threshold acceptance algorithm (79). Further savings can be attained by developing strategies that exploit the fact that pixel interchanges are local and thus one can reuse the correlation functions measured in the previous time step instead of recomputing them fully at any step (78). Additional cost savings have been achieved by interchanging pixels only at the two-phase interface (107). The reader is referred to the aforementioned references for additional details.

Illustrative Examples

Lower-order correlation functions generally do not contain complete information and thus cannot be expected to yield perfect reconstructions. Of course, the

judicious use of combinations of lower-order correlation functions can yield more accurate reconstructions than any single function alone. Yeong & Torquato (76, 78) clearly showed that the two-point function S_2 alone is not sufficient to accurately reconstruct random media. By also incorporating the lineal-path function L, they were able to obtain better reconstructions. They studied one-, two-, and three-dimensional digitized isotropic media. Each simulation began with an initial configuration of pixels (white for phase 1 and black for phase 2) in the random checkerboard arrangement at a prescribed volume fraction.

A two-dimensional example illustrating the insufficiency of S_2 in reconstructions is a target system of overlapping disks at a disk volume fraction of $\phi_2 = 0.5$; see Figure 14*a*. Reconstructions that accurately match S_2 alone, L alone, and both S_2 and L are shown in Figure 14. The S_2-reconstruction is not very accurate; the

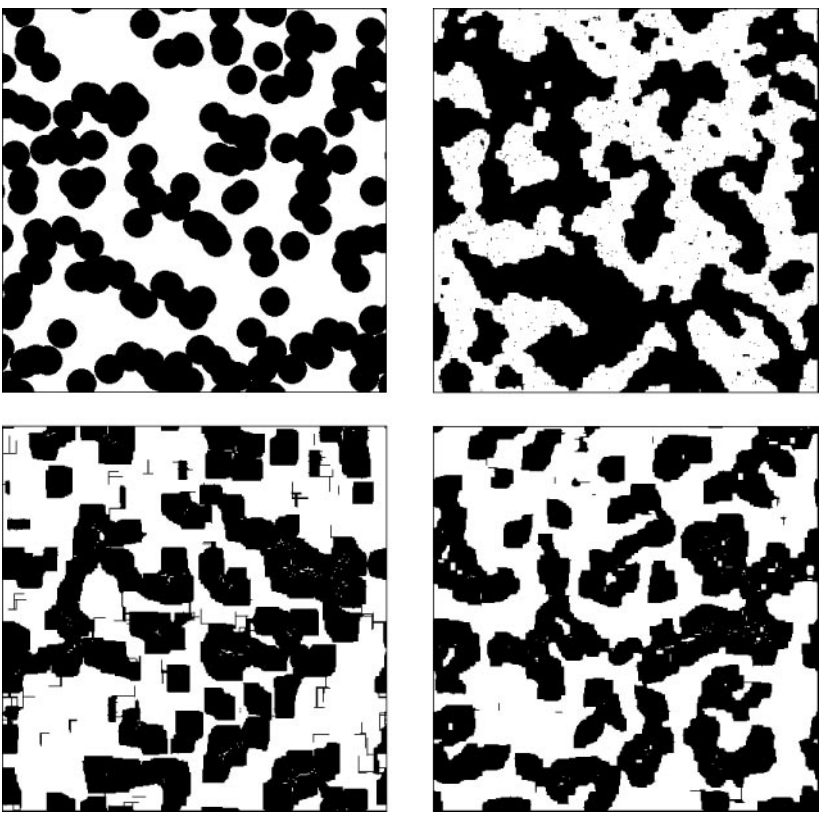

Figure 14 (*a*) Target system: a realization of random overlapping disks. System size $= 400 \times 400$ pixels, disk diameter $= 31$ pixels, and volume fraction $\phi_2 = 0.5$. (*b*) S_2-reconstruction. (*c*) Corresponding L-reconstruction. (*d*) Corresponding hybrid $(S_2 + L)$-reconstruction.

cluster sizes are too large, and the system actually percolates (note that overlapping disks percolate at a disk area fraction of $\phi_2 \approx 0.68$ (1). The L-reconstruction does a better job than the S_2-reconstruction in capturing the clustering behavior. However, the hybrid ($S_2 + L$)-reconstruction is the best.

The optimization method can be used in the construction mode to find the specific structures that realize a specified set of correlation functions. An interesting question in this regard is the following: Is any correlation function physically realizable or must the function satisfy certain conditions? It turns out that not all correlation functions are physically realizable. For example, what are the existence conditions for a valid (i.e., physically realizable) autocovariance function $\chi(\boldsymbol{r}) \equiv S_2^{(i)}(\boldsymbol{r}) - \phi_i^2$ for statistically homogeneous two-phase media? There are certain nonnegativity conditions involving the spectral representation of the autocovariance $\chi(\boldsymbol{r})$ that must be obeyed (96). However, it is not well known that these nonnegativity conditions are necessary but not sufficient conditions that a valid autocovariance $\chi(\boldsymbol{r})$ of a statistically homogeneous two-phase random medium (i.e., a binary stochastic spatial process) must meet. Some of these binary conditions are described by Torquato (1), but the complete characterization is a very difficult problem. Suffice it to say that the algorithm in the construction mode can be used to provide guidance on the development of the mathematical conditions that a valid autocovariance $\chi(\boldsymbol{r})$ must obey.

Cule & Torquato (79) considered the construction of realizations having the following autocovariance function:

$$\frac{S_2(r) - \phi_1^2}{\phi_1 \phi_2} = e^{-r/a} \frac{\sin(qr)}{qr}, \qquad 31.$$

where $q = 2\pi/b$ and the positive parameter b is a characteristic length that controls oscillations in the term $\sin(qr)/(qr)$, which also decays with increasing r. This function possesses phase-inversion symmetry and exhibits a considerable degree of short-range order; it generalizes the purely exponentially decaying function studied by Debye and coworkers (108). This function satisfies the nonnegativity condition on the spectral function but may not satisfy the binary conditions, depending on the values of a, b, and ϕ_1 (96). Two structures possessing the correlation function (31) are shown in Figure 15 for $\phi_2 = 0.2$ and 0.5, in which $a = 32$ pixels and $b = 8$ pixels. For these sets of parameters, all of the aforementioned necessary conditions on the function are met. At $\phi_2 = 0.2$, the system resembles a dilute particle suspension with particle diameters of order b. At $\phi_2 = 0.5$, the resulting pattern is labyrinthine such that the characteristic sizes of the "patches" and "walls" are of order a and b, respectively. $S_2(r)$ was sampled in all directions during the annealing process. In all of the previous two-dimensional examples, however, both S_2 and L were sampled along the two principal directions in order to save computational time. This time-saving step should be implemented only for isotropic media, provided that there is no appreciable short-range order; otherwise, it leads to unwanted anisotropy (79, 109). However, this artificial anisotropy can be significantly reduced by optimizing along four selected directions on a square lattice (110).

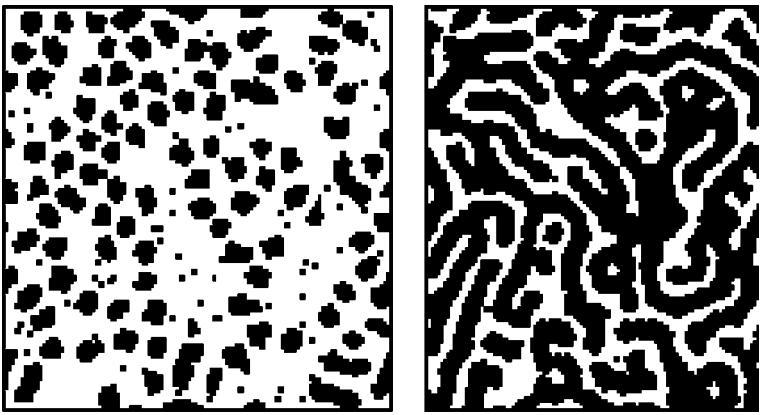

Figure 15 Structures corresponding to the target correlation function given by (31) for $\phi_2 = 0.2$ and 0.5. Here $a = 32$ pixels and $b = 8$ pixels.

To what extent can information extracted from two-dimensional cuts through a three-dimensional isotropic medium, such as S_2 and L, be employed to reproduce intrinsic three-dimensional information, such as connectedness? This question was studied in the aforementioned Fontainebleau sandstone for which we know the full three-dimensional structure via X-ray microtomography (76). The three-dimensional reconstruction that results by using a single slice of the sample and matching both S_2 and L is shown in Figure 16. The reconstructions accurately reproduce certain three-dimensional properties of the pore space, such as the pore-size functions, the mean survival time of a Brownian particle, and the fluid permeability. The degree of connectedness of the pore space also compares remarkably well with the actual sandstone, although this is not always the case (111).

CONCLUSIONS

A macroscopic or effective property of a material is a function of the relevant local fields weighted with certain correlation functions that statistically characterize the structure. Generally, the type of correlation function involved depends on the specific physical problem that one studies. However, for certain classes of materials, it has been shown that all of the apparently different types of correlation functions can be obtained from a canonical function H_n and, consequently, can be shown to be related to one another. Such a unified approach to studying macroscopic properties of disordered materials is both natural and very powerful. Nonetheless, many challenges remain. For example, the extension of these ideas to characterize molecular systems with directional bonding has yet to be developed. A systematic means of incorporating into structure/property relations important

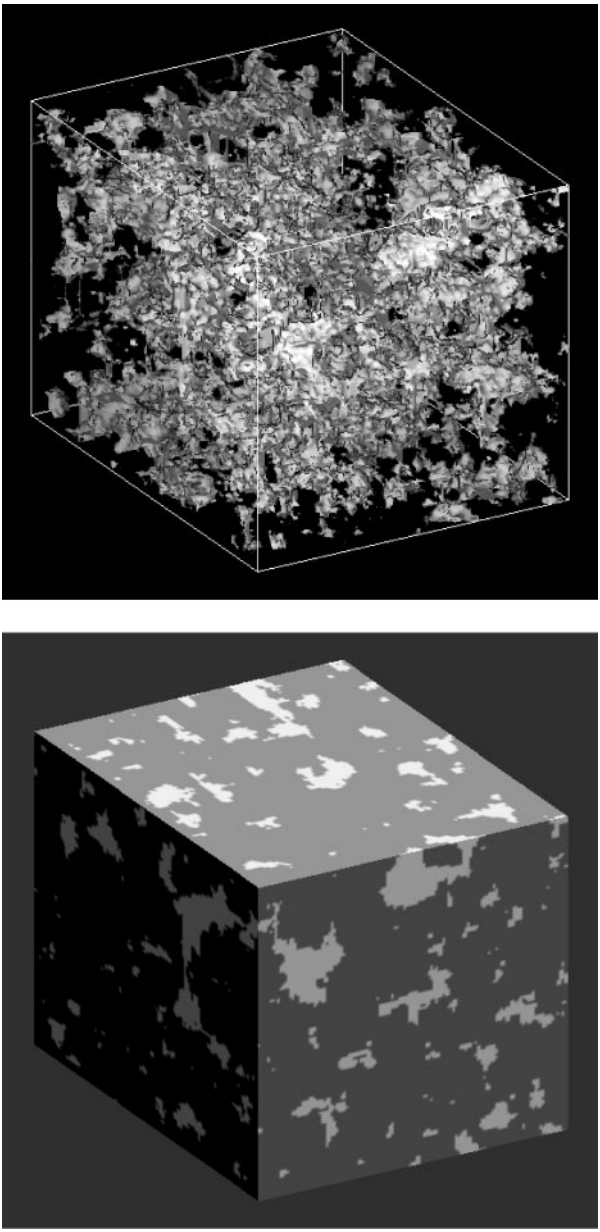

Figure 16 Hybrid reconstruction of the sandstone shown in Figure 10 using both S_2 and L obtained from a single "slice." System size is $128 \times 128 \times 128$ pixels. (*Top*) Pore space is white and opaque, and the grain phase is black and transparent. (*Bottom*) Three-dimensional perspective of the surface cuts.

topological information, such as connectedness, has not been accomplished to date.

The characterization of disordered materials via order metrics is in its infancy. The use of scalar order metrics to characterize the degree of randomness in materials of general structure and composition has heretofore not been investigated. The appropriate order metrics will depend on the types of material structures of interest. The successful quantification of structures in order-metric space may potentially be employed to categorize classes of disordered materials. Moreover, such analyses will enable one to place the equilibrium and nonequilibrium (or history-dependent) states of molecular systems in order-metric space.

The stochastic optimization technique is a promising new way to reconstruct or construct disordered materials. However, its full potential and limitations have yet to be fully explored. Many of the fascinating questions and issues identified above remain open.

ACKNOWLEDGMENTS

This work has been supported by the Office of Basic Energy Sciences at the U.S. Department of Energy and the Petroleum Research Fund administered by the American Chemical Society.

The *Annual Review of Materials Research* is online at http://matsci.annualreviews.org

LITERATURE CITED

1. Torquato S, 2002. *Random Heterogeneous Materials: Microstructure and Macroscopic Properties*. New York: Springer-Verlag. 701 pp.
2. Torquato S, Yeong CLY, Rintoul MD, Milius D, Aksay IA. 1999. *J. Am. Ceram. Soc.* 82:1263–68
3. Coker DA, Torquato S, Dunsmuir JH. 1996. *J. Geophys. Res.* 101:17497–506
4. Torquato S, Truskett TM, Debenedetti PG. 2000. *Phys. Rev. Lett.* 84:2064–67
5. Torquato S, Stell G. 1982. *J. Chem. Phys.* 77:2071–77
6. Brown WF. 1955. *J. Chem. Phys.* 23: 1514–17
7. Beran MJ. 1968. *Statistical Continuum Theories*. New York: Wiley. 424 pp.
8. Milton GW. 1981. *J. Appl. Phys.* 52:5294–304
9. Phan-Thien N, Milton GW. 1982. *Proc. R. Soc. London Ser. A* 380:333–48
10. Torquato S. 1985. *J. Appl. Phys.* 58:3790–97
11. Willis JR. 1977. *J. Mech. Phys. Solids* 25: 185–202
12. Milton GW. 1982. *J. Mech. Phys. Solids* 30:177–91
13. Milton GW, Phan-Thien N. 1982. *Proc. R. Soc. London Ser. A* 380:305–31
14. Torquato S, 1997. *Phys. Rev. Lett.* 79:681–84
15. Torquato S, Rubinstein J. 1989. *J. Chem. Phys.* 90:1644–47
16. Prager S. 1961. *Phys. Fluids* 4:1477–82
17. Berryman JG, Milton GW. 1985. *J. Chem. Phys.* 83:754–60
18. Rubinstein J, Torquato S. 1989. *J. Fluid Mech.* 206:25–46

19. Debye P, Bueche AM. 1949. *J. Appl. Phys.* 20:518–25
20. Doi M. 1976. *J. Phys. Soc. Jpn.* 40:567–72
21. Rubinstein J, Torquato S. 1988. *J. Chem. Phys.* 88:6372–80
22. Lu BL, Torquato S. 1992. *Phys. Rev. A* 45:922–29
23. Matheron G. 1975. *Random Sets and Integral Geometry*. New York: Wiley
24. Torquato S, Lu B. 1993. *Phys. Rev. E* 47: 2950–53
25. Ho FG, Strieder W. 1979. *J. Chem. Phys.* 70:5635–39
26. Tokunaga TK. 1985. *J. Chem. Phys.* 82: 5298–99
27. Tassopoulos M, Rosner DE. 1992. *Chem. Eng. Sci.* 47:421–43
28. Thompson AH, Katz AJ, Krohn CE. 1987. *Adv. Phys.* 36:625–94
29. Underwood EE. 1970. *Quantitative Stereology*. Reading, MA: Addison-Wesley. 274 pp.
30. Prager S. 1963. *Chem. Eng. Sci.* 18:227–31
31. Torquato S, Beasley JD, Chiew YC. 1988. *J. Chem. Phys.* 88:6540–46
32. Keller JB, Rubenfeld L, Molyneux J. 1967. *J. Fluid Mech.* 30:97–125
33. Chandrasekhar S. 1943. *Rev. Mod. Phys.* 15:1–89
34. McNally JG, Cox EC. 1989. *Development* 105:323–33
35. Reiss H, Frisch HL, Lebowitz JL. 1959. *J. Chem. Phys.* 31:369–80
36. Bernal JD. 1964. *Proc. R. Soc. London Ser. A* 280:299–322
37. Finney JL. 1970. *Proc. R. Soc. London Ser. A* 319:479–93
38. Zallen R. 1983. *The Physics of Amorphous Solids*. New York: Wiley. 304 pp.
39. Torquato S, Lu B, Rubinstein J. 1990. *Phys. Rev. A* 41:2059–75
40. Hertz P. 1909. *Math. Ann.* 67:387–98
41. Hefland E, Reiss H, Frisch HL, Lebowitz JL. 1960. *J. Chem. Phys.* 33:1379–85
42. Torquato S. 1986. *J. Chem. Phys.* 84: 6345–59
43. Quintanilla J, Torquato S. 1995. *J. Appl. Phys.* 77:4361–72
44. Torquato S, Beasley JD. 1987. *Phys. Fluids* 30:633–41
45. Torquato S, Rintoul MD. 1995. *Phys. Rev. Lett.* 75:4067–70. Erratum. 1996. *Phys. Rev. Lett.* 76:3241
46. Torquato S. 1986. *J. Stat. Phys.* 45:843–73
47. Boltzmann L. 1898. *Lectures on Gas Theory*. Transl. SG Brush, 1964. Berkeley, CA: Univ. Calif. Press
48. Stell G. 1966. Boltzmann's method of evaluating and using molecular distribution functions. *Tech. Rep*. Brooklyn Polytechnic Inst.
49. Torquato S, Stell G. 1983. *J. Chem. Phys.* 78:3262–72
50. Stell G. 1985. Mayer-Montroll equations (and some variants) through history for fun and profit. In *The Wonderful World of Stochastics: A Tribute to Elliott W. Montroll*, ed. MF Shlesinger, GH Weiss. New York: Amsterdam
51. Lu BL, Torquato S. 1991. *Phys. Rev. A* 43:2078–80
52. Torquato S, Sen AK. 1990. *J. Appl. Phys.* 67:1145–55
53. Quintanilla J, Torquato S. 1996. *Phys. Rev. E* 53:4368–78
54. Lu BL, Torquato S. 1990. *Phys. Rev. B* 42:4453–59
55. Hansen JP, McDonald IR. 1986. *Theory of Simple Liquids*. New York: Academic. 556 pp.
56. Rintoul MD, Torquato S. 1996. *Phys. Rev. Lett.* 77:4198–201
57. Russel WB, Saville DA, Schowalter WR. 1989. *Colloidal Dispersions*. Cambridge, UK: Cambridge Univ. Press
58. Torquato S, Lado F. 1988. *Proc. R. Soc. London Ser. A* 417:59–80
59. Torquato S, Lado F. 1986. *Phys. Rev. B* 33:6428–34
60. Metcalfe G, Shinbrot T, McCarthy JJ, Ottino JM. 1995. *Nature* 374:39–41
61. Widom B. 1966. *J. Chem. Phys.* 44:3888–94

62. Reńyi A. 1963. *Sel. Trans. Math. Stat. Prob.* 4:203–18
63. Feder J. 1980. *J. Theor. Biol.* 87:237–54
64. Cooper DW. 1988. *Phys. Rev. A* 38:522–24
65. Baxter RJ. 1968. *Austr. J. Phys.* 21:563–69
66. Torquato S, Stell G. 1983. *J. Chem. Phys.* 79:1505–10
67. Torquato S, Stell G. 1985. *J. Chem. Phys.* 82:980–87
68. Torquato S, Avellaneda M. 1991. *J. Chem. Phys.* 95:6477–89
69. Corson PB. 1974. *J. Appl. Phys.* 45:3159–64
70. Corson PB. 1974. *J. Appl. Phys.* 45:3165–70
71. Flegler SL, Heckman JW, Klomparens KL. 1993. *Scanning and Transmission Electron Microscopy: An Introduction*. New York: Freeman
72. Stroscio JA, Kaiser WJ. 1993. *Scanning Tunneling Microscopy*. New York: Academic
73. Kinney JH, Nichols MC. 1992. *Annu. Rev. Mater. Sci.* 22:121–52
74. Howle LE, Behringer RP, Georgiadis JG. 1993. *Nature* 362:230–32
75. Fredrich JT, Menendez B, Wong TF. 1995. *Science* 268:276–79
76. Yeong CLY, Torquato S. 1998. *Phys. Rev. E* 58:224–33
77. Coker DA, Torquato S. 1995. *J. Appl. Phys.* 77:6087–99
78. Yeong CLY, Torquato S. 1998. *Phys. Rev. E* 57:495–506
79. Cule D, Torquato S. 1999. *J. Appl. Phys.* 86:3428–37
80. Berryman JG. 1985. *J. Appl. Phys.* 57: 2374–84
81. Berryman JG, Blair SC. 1986. *J. Appl. Phys.* 60:1930–38
82. Berryman JG. 1989. Estimating effective moduli of composites using quantitative image analysis in random media and composites. In *Random Media and Composites*, ed. RV Kohn, GW Milton. Philadelphia: SIAM
83. Hoshen J, Kopelman R. 1976. *Phys. Rev. B* 14:3438–45
84. Sevick EM, Monson PE, Ottino JM. 1988. *J. Chem. Phys.* 88:1198–211
85. Kittel C. 1996. *Introduction to Solid State Physics*. New York: Wiley
86. Cusack NE. 1987. *The Physics of Structurally Disordered Matter: An Introduction*. Bristol, CT: Higler
87. Bernal JD. 1965. The geometry of the structure of liquids. In *Liquids: Structure, Properties, Solid Interactions*, ed. TJ Hughel, pp. 25–50. New York: Elsevier
88. Gotoh K, Finney JL. 1974. *Nature* 252: 202–5
89. Berryman JG. 1983. *Phys. Rev. A* 27: 1053–61
90. Steinhardt PJ, Nelson DR, Ronchetti M. 1983. *Phys. Rev. B* 28:784–805
91. Truskett TM, Torquato S, Debenedetti PG. 2000. *Phys. Rev. E* 62:993–1001
92. Kansal AR, Truskett TM, Torquato S. 2000. *J. Chem. Phys.* 113:4844–51
93. Torquato S, Stillinger FH. 2002. *Phys. Rev. E*. Submitted
94. Lubachevsky BD, Stillinger FH. 1990. *J. Stat. Phys.* 60:561–83
95. Errington JR, Debenedetti PG. 2001. *Nature* 409:318–21
96. Torquato S. 1999. *J. Chem. Phys.* 111: 8832–37
97. Rice SO. 1944. *Bell. Syst. Tech.* 23:282–332
98. Joshi MY. 1974. *A class of stochastic models for porous media*. PhD thesis. Univ. Kansas, Lawrence
99. Quibler JA. 1984. *J. Colloid Interface Sci.* 98:84–102
100. Adler PM. 1992. *Porous Media—Geometry and Transports*. Boston: Butterworth-Heinemann
101. Cahn JW. 1965. *J. Chem. Phys.* 42:93–99
102. Berk NF. 1987. *Phys. Rev. Lett.* 58:2718–21
103. Teubner M. 1991. *Europhys. Lett.* 14:403–8

104. Roberts AP, Teubner M. 1995. *Phys. Rev. E* 51:4141–54
105. Rintoul MD, Torquato S. 1997. *J. Colloid Interface Sci.* 186:467–76
106. Horst R, Pardalos PM. 1995. *Handbook of Global Optimization*. New York: Kluwer
107. Rozman MG, Utz M. 2001. *Phys. Rev. E* 63:066701:1–8
108. Debye P, Anderson HR, Brumberger H. 1957. *J. Appl. Phys.* 28:679–83
109. Manwart C, Hilfer R. 1999. *Phys. Rev. E* 59:5596–99
110. Sheehan N, Torquato S. 2001. *J. Appl. Phys.* 89:53–60
111. Manwart C, Torquato S, Hilfer R. 2000. *Phys. Rev. E* 62:893–99

Annual Review of Materials Research
Volume 32, 2002

CONTENTS

COMPUTATIONAL MATERIALS RESEARCH